C. R. Geoscience 349 (2017) 96–105

Contents lists available at ScienceDirect

Comptes Rendus Geoscience

www.sciencedirect.com

Internal Geophysics

Intraplate earthquakes and their link with mantle dynamics: Insights from P-wave teleseismic tomography along the northern part of the North–South Tectonic Zone in China

Chuansong He [a,*], M. Santosh [b,c]

[a] China Earthquake Administration, Institute of Geophysics, 100081 Beijing, China
[b] Department of Earth Sciences, Centre for Tectonics, Exploration and Resources, University of Adelaide, 5005 Adelaide, SA, Australia
[c] School of Earth Sciences and Resources, China University of Geosciences Beijing, 29, Xueyuan Road, 100083 Beijing, China

ARTICLE INFO

Article history:
Received 19 March 2017
Accepted after revision 10 April 2017
Available online 17 May 2017

Handled by Michel Campillo

Keywords:
Earthquakes
Upper mantle
P-wave teleseismic tomography
Crustal and lithospheric delamination
North-South Tectonic Zone

ABSTRACT

The North–South Tectonic Zone (NSTZ) running across the Chinese continent is an important earthquake-prone zone. Around one third of the strong earthquakes (> 7.0) of China in the past occurred in this region. Receiver function study has imaged vertical convection in the mantle beneath the northern part of the NSTZ (NNSTZ), which might be related to stress accumulation and release as well as related earthquakes. Here we perform a P-wave teleseismic tomographic analysis of this region. Our results reveal prominent low-velocity and high-velocity perturbations in the upper mantle beneath this region, which we correlate with mantle upwelling, possibly resulting from lower crustal and (or) lithospheric delamination. Our results also reveal significant contrast in the velocity perturbation of the lithosphere along the two sides of this tectonic zone, suggesting possible material exchange between the eastern and western domains and lithosphere-scale control on the generation of earthquakes.

1. Introduction

The northern part of the North-South Tectonic Zone in China (NNSTZ), located along 102°–106° east longitude, includes the Alashan block, Yinshan block, Qilian block, Ordos block, Qaidam block, Songpan-Ganzi block, South China block, and Qinling orogenic belt (Fig. 1) (He et al., 2014; Li et al., 2006; Zhang and Wang, 2009; Zhang et al., 2013). This zone divides China into an eastern segment with a crustal thickness of 30–44 km and a western segment with a thickness of 54–70 km (He et al., 2014; Li et al., 2006) with a strong lateral gradient in crustal thickness and north–south-trending gravity anomaly (He et al., 2014; Li et al., 2006; Zhang et al., 2013).

The NNSTZ preserves a complex tectonic history. In its eastern side, the Ordos and Yinshan blocks amalgamated at ca. 1.95 Ga (Dan et al., 2012; Zhao et al., 2010). The collision zone between the two blocks is popularly known as the Khondalite Belt or the Inner Mongolia Suture Zone (Santosh, 2010; Santosh et al., 2007, 2013; Zhao et al., 2005). The Ordos basin (within the Ordos block) in central China is a large intracratonic compressional basin (Li, 1996; Wang et al., 2005), and its tectonic evolution was affected by both the Triassic collision between North and

* Corresponding author.
E-mail address: hechuansong@aliyun.com (C. He).

http://dx.doi.org/10.1016/j.crte.2017.04.002
1631-0713/

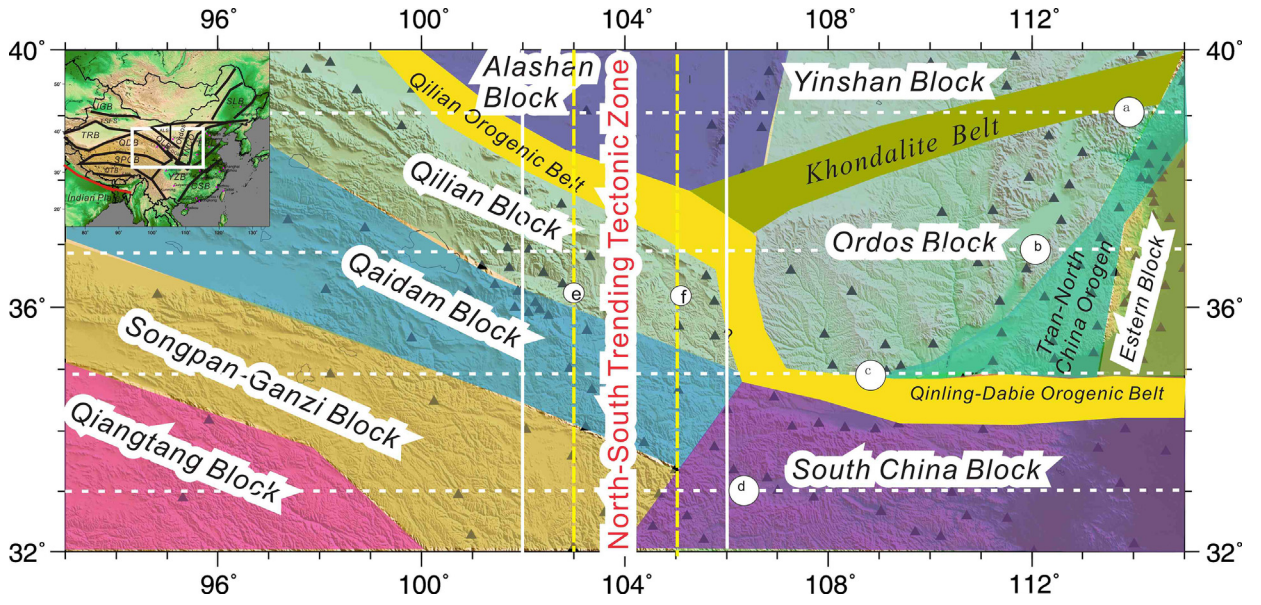

Fig. 1. Tectonic framework in the NNSTZ and near-by area showing profiles for the velocity perturbation (a–f profiles). Black triangle: seismic station. Insert figure (upper left corner): the study area within the East Asian region (marked by box). SLB (Songliao Basin), WBL (Western Block), EBL (Eastern Block), TNCO (Tans North China Orogen), Q-DOB (Qinling–Dabie Orogen Belt), YZB (Yangtze Block or South China Block), CSB (Cathaysia Block), JGB (Junggar Basin), TSFS (Tianshan Fold System), TRB (Tarim Basin), QDB (Qaidam Block), SPGB (Songpan–Ganzi Block), QLB (Qilian Block), QTB (Qiangtang Block), ALS (Alashan Block).

South China Blocks (Ames et al., 1996; Ratschbacher et al., 2000) and the subduction of the Pacific plate since the Mesozoic (Yin and Nie, 1996). In the western part of NNSTZ, the Qilian orogenic belt along the northern margin of the Tibetan Plateau of Caledonian age was formed by the convergence and collision of the Alxa, Qilian and Qaidam blocks during Late Ordovician to Devonian (Xu et al., 2006, 2010). Among these blocks, the Qilian-Qaidam blocks are considered to represent a composite fragment of the Neoproterozoic Rodinia supercontinent and shows affinity with the Yangtze craton in South China (Song et al., 2010). The Kunlun and Qilian orogenic belts represent a suture zone marking the closure of the Proto-Tethyan Ocean (Bian et al., 2004; Tseng et al., 2009; Tung et al., 2007; Xiao et al., 2015).

The critical tectonic feature and cause of frequent earthquakes along the NNSTZ (Deng et al., 2003; Zhang et al., 2003) has been the topic of a series of geophysical studies along this zone in the last decades, such as deep seismic sounding (e.g., Gao et al., 2006; Li et al., 2002), tomography, receiver function and shear-wave splitting (e.g., Ding et al., 1999; He et al., 2014; Liu et al., 1989; Wang et al., 2008), etc. These investigations revealed the crustal and lithospheric structure as well as the upper mantle structure. However, the possible link between the earthquake-prone region and deep continental dynamics has not been well elucidated.

In this study, we employed P-wave teleseismic tomography to evaluate the velocity structure of the lithosphere and upper mantle. Based on tomographic results, in conjunction with those from our previous study (He et al., 2014), we attempt to evaluate the geodynamic processes beneath the NNSTZ in order to gain insights on the relationship between the deep dynamic process and earthquake initiation.

2. Data and method

In the modeling space, a 3-D grid is set up and Vp (P-wave velocity) perturbations at the grid nodes are taken as unknown parameters. The Vp perturbation at any point in the model is calculated by linearly interpolating the Vp perturbations at the eight grid nodes surrounding that point. In our optimal Vp model, the lateral grid interval is 1°, and grid meshes are set at depths of 70, 100, 200, 300, 400, 500, 600, 700, and 800 km. An efficient 3-D ray-tracing technique (Zhao et al., 1992) is used to calculate theoretical travel times and ray paths. A conjugate-gradient inversion algorithm (Paige and Saunders, 1982) with damping and smoothing regularizations is adopted to solve the large and sparse system of observation equations (Zhao et al., 1992, 1994, 2002). The iasp91 1-D Earth model (Kennett and Engdahl, 1991) is taken as the starting model for the 3-D tomographic inversion (e.g., Lei and Zhao, 2007; Yang et al., 2014; Zhao et al., 1992).The first P-wave arrival times are picked from the origin seismograms of teleseismic events (Fig. 2). Travel-time residuals (t_{ij}) are determined by subtracting theoretical travel times and origin times from the observed arrival times. It can be expressed as:

$$t_{ij} = T_{ij}^{OBS} - T_{ij}^{CAL} \quad (1)$$

From the j-th event to the i-th station, where T_{ij}^{OBS} and T_{ij}^{CAL} are the observed and calculated travel times, respectively.Following this, the relative travel-time residuals (r_{ij}) are obtained by subtracting the mean travel-time residual of

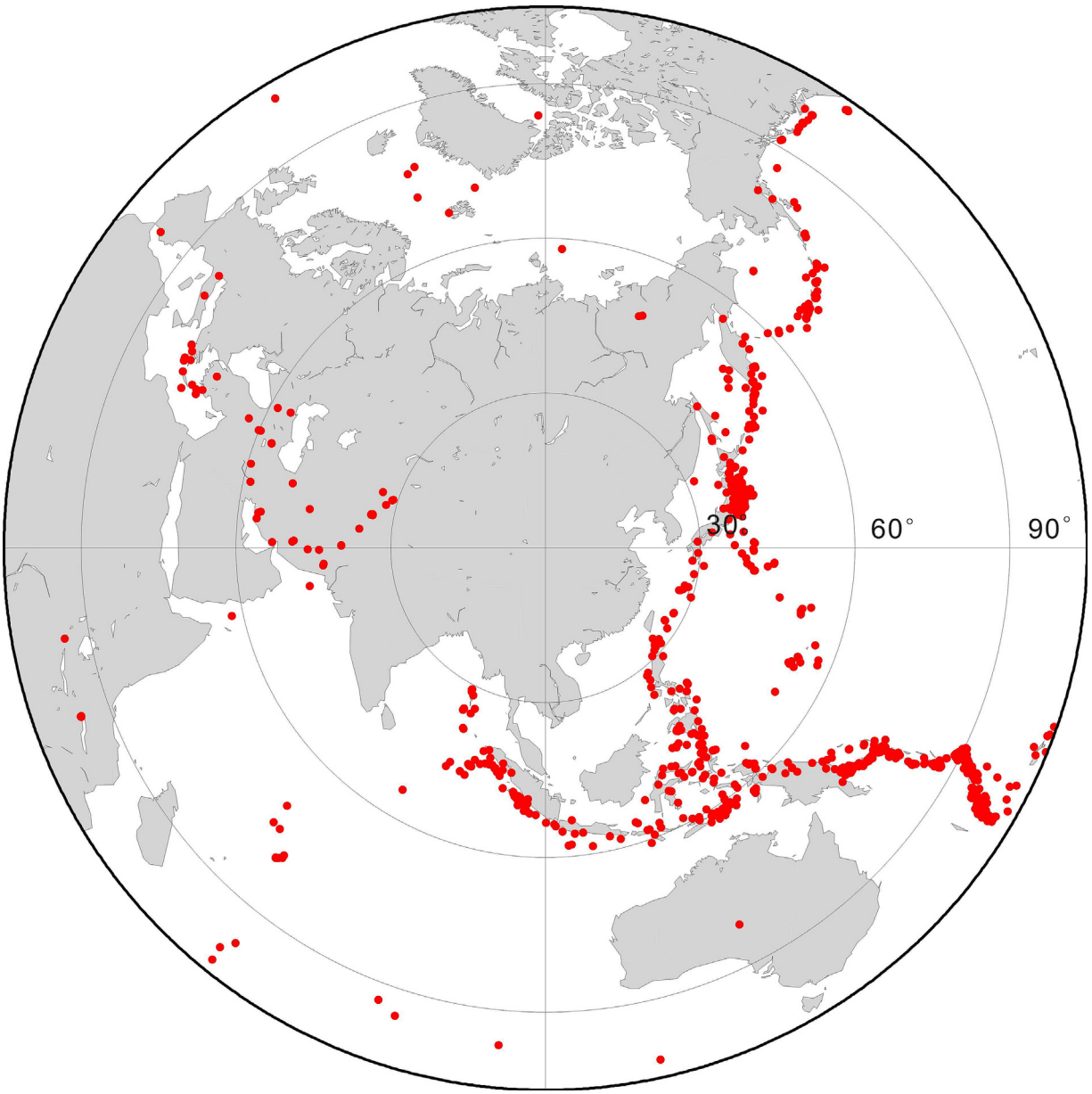

Fig. 2. Earthquake events (red circle) that were used for tomographic inversion, recorded between July 2007 and March 2014 with epicenter distance ranging from 30° to 85° for each station-event pair.

each teleseismic event from the raw residuals. The relative residuals are inverted for a 3-D Vp model beneath the study region, thus the effects of hypocentral mislocations of the teleseismic events and structural heterogeneities outside the modeling space can be greatly reduced (Zhao et al., 1994). The r_{ij} are expressed as:

$$r_{ij} = t_{ij} - t_j^{\mathrm{m}} \tag{2}$$

where $t_j^{\mathrm{m}} = \frac{1}{n_j}\sum_{i=1}^{n_j} t_{ij}$ is the average residual, and n_j is the number of observations for the j-th event.

In this study, we collected data recorded by China seismic network between July 2007 and March 2014, which comprise 203 seismic stations and the 325 events that were selected with epicentral distance ranging from 30°–85 °correspond to an earthquake magnitude >6.0 (Fig. 2). *P* arrivals were correlated on the vertical component after bandpass filtering between 0.3 and 3 Hz. Our assembled data set contains 40330 *P*-wave arrivals from these events. The data of great than −2 s and less than 2 s were selected to use tomographic inversion (Fig. S1).

In teleseismic tomography, rays do not crisscross well in the crust and the uppermost mantle beneath the study region. Therefore, the effect of crustal heterogeneity should be removed through correcting the relative

travel-time residuals, which is called crustal correction (Jiang et al., 2009, 2015). We calculated the crustal correction for the upper 70 km of the earth, which is the upper depth limit of tomography. In this work, the CRUST1.0 model (Laske et al., 2012) is used to apply the crustal correction to the relative travel-time residuals following the scheme of Jiang et al. (2009, 2015).

In order to obtain a balance between the reduction of travel time residuals and the smoothness of the 3-D velocity structure (Eberhart-Phillips, 1986; Huang et al., 2015; Lei and Zhao, 2007), we carried out a series of inversion tests with different values of damping, and eventually selected the optimal value of damping parameter as 15 (Fig. S2).

In the checkerboard resolution test, we also designed the grid spacing as $1^\circ \times 1^\circ$ and the vertical grid spacing as 70, 100, 200, 300, 400, 500, 600, 700, and 800 km, respectively. Positive and negative velocity perturbations of 5% were assigned to all the 3-D grid nodes and synthetic travel times were calculated by tracing the rays for the checkerboard so that we can evaluate the adequacy of ray coverage and reliability of the main features of the tomographic images (e.g., Wang and Zhao, 2013; Zhao et al., 1992). Following this method, the synthesized data were inverted to evaluate whether the assigned checkerboard pattern could be recovered or not. The results show that the resolution is generally high in most parts of the study area such as 100, 200, 300, 400, 500 and 600 km depth sections (Fig. S3) except for the western part, whereas in the 70, 700 and 800 km depth sections, the resolution is low. We also launched the checkerboard resolution test for four east–west profiles and two north–south profiles, and the results show high resolution along most part of the east–west profile sections, except for the western part and the marginal domain (Fig. S4), and high resolution along most parts of north–south profiles, except for the marginal domain (Fig. S5).

3. Results

The tomography results show a large-scale low-velocity perturbation (Lv1) beneath the western side of the NNSTZ at 70, 100, 200, 300 km depth sections, whereas a large-scale high-velocity perturbation (Hv1) is seen at 70, 100 and 200 km depth sections in the eastern side of the NNSTZ (Fig. 3). A previous shear-wave tomographic study also identified a low-velocity structure beneath the western side of the NNSTZ, whereas the eastern side is characterized by high-velocity structure at 100 km depth (Pandey et al., 2014). Other P-wave teleseismic tomographic studies also demonstrate low-velocity perturbation along the western side and high-velocity perturbation to the eastern side of the NNSTZ at 70, 120, 140, 160, 200 and 300 km depth (Li et al., 2006; Tian et al., 2009; Wang et al., 2015). In the 300 km depth section, there is a high-velocity perturbation (Hv2) at south part of the NNSTZ and a large-scale low-velocity perturbation at the eastern side of the NNSTZ (Lv2) (Fig. 3). In the 400- and 500-km depth sections, there is discontinuous high-velocity perturbation (Hv3) (Fig. 3). In the 500- and

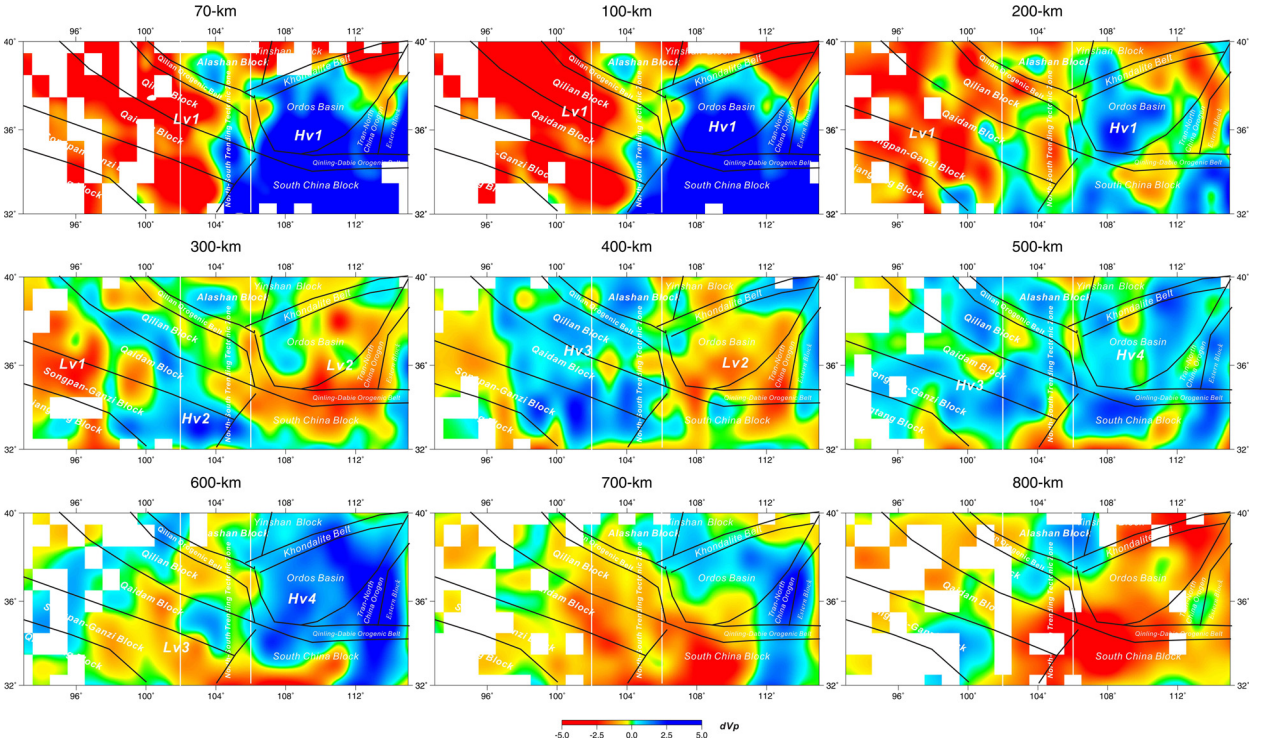

Fig. 3. P-wave velocity perturbations at 70, 100, 200, 300, 400, 500, 600, 700 and 800 km detpth sections relative to iasp91 1D velocity model (Kennett and Engdahl, 1991). We hide portions of the model where the recovery of the starting model in the CRT was below 10% (Fig. S3).

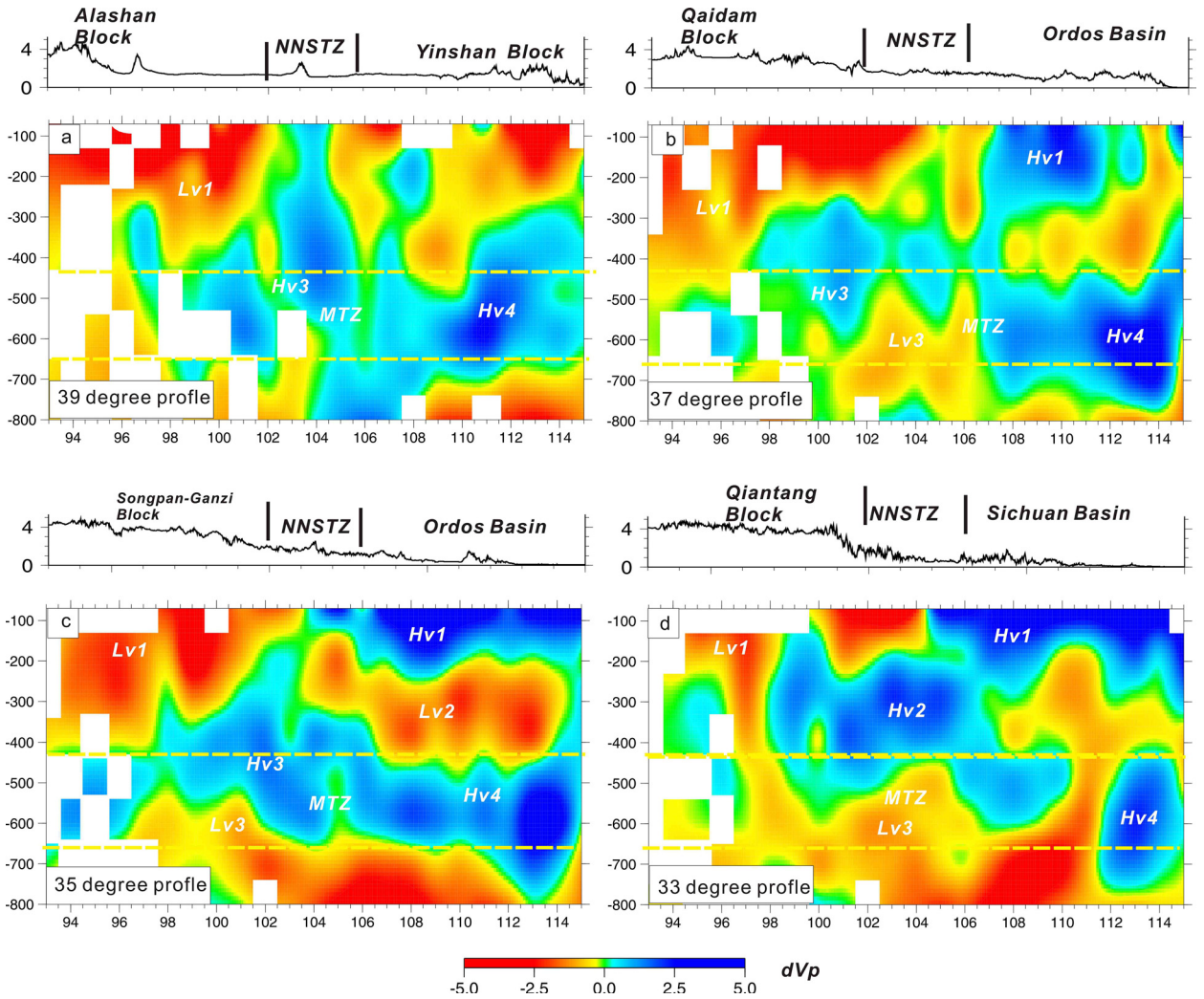

Fig. 4. Velocity perturbation along the west–east profiles. We hide the portions of the model where the recovery of the starting model in the CRT was below 10% (Fig. S4). NNSTZ: North part of North-South Tectonic Zone. Tomographic results reveal high-velocity perturbation in the eastern side of the NNSTZ and low-velocity perturbation in the western side of the NNSTZ at the lithospheric scale. The discontinuous high-velocity perturbation (Hv3 and Hv4) in the upper mantle and mantle transition zone may be associated with the crustal and lithospheric delamination, which resulted in mantle upwelling or large-scale low-velocity perturbation (Lv2) in the upper mantle.

600-km depth sections, there is a large-scale high-velocity perturbation (Hv4) at the eastern side of the NNSTZ (Fig. 3). The velocity structure at depth sections of 700 and 800 km depth sections are mostly inferred due to lower resolution, and we exclude these from further discussion on the depth sections.

In order to further check the above results, we performed four east–west profiles (see Fig. 1 for profile location, and Fig. 4) and two north–south profiles (see Fig. 1 for profile location, and Fig. 5). The results show a large-scale low-velocity perturbation (Lv1) in the upper mantle beneath the western side of the NNSTZ (Fig. 4a–d), whereas in the eastern side, there is a large-scale high-velocity perturbation (Hv1) (Fig. 4b–d). At the same time, the high-velocity perturbation (Hv3 and Hv4) can be clearly seen at all profile in the mantle transition zone (Fig. 4). The Hv2 is beneath the NNSTZ and at about 300–400 km in depth (Fig. 4d). The north–south profiles show a high-velocity perturbation (Hv3) in the mantle transition zone and another high-velocity perturbation (Hv2) at 300–400 km beneath the southern part of the NNSTZ (Fig. 5), and a low-velocity perturbation (Lv2) at 300–400 km in depth beneath the NNSTZ (Fig. 5f).

4. Discussion

The plate boundaries are the major regions of magmatism, metamorphism, deformation and tectonics including major earthquakes associated with oceanic plate subduction or continental collision. However, recent studies reveal that micro-continental boundaries, palaeosuture zones, mobile belts and ancient deformation zones play a critical role intra-plate tectonics (e.g., Aitken et al., 2013; Gorczyk and Vogt, 2015). Especially, the compressed

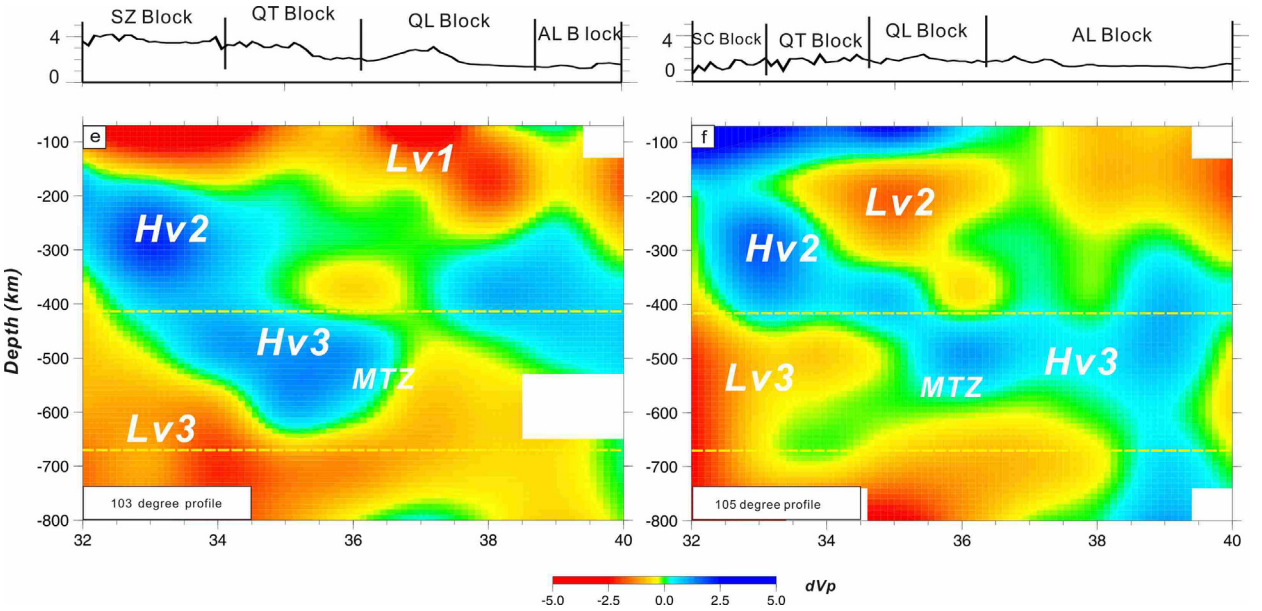

Fig. 5. North–south profiles for the velocity perturbation (see Fig. 1 for profile location); a and b are 103° and 105° profiles, respectively (see Fig. 1 for profile location). We hide portions of the model where the recovery of the starting model in the CRT was below 10% (Fig. S5). The prominent high-velocity perturbation in the upper mantle and mantle transition zone (Hv2 and Hv3) and low-velocity perturbation at 300–400 km in depth (Lv2). SZ block: Songpan-Ganzi block, QT block: Qaidam block, QL block: Qilian block, AL block: Alashan block, SC block: south China block.

lithosphere can develop a wide range of lateral heterogeneities in such settings, leading to magmatism, deformation, metallogeny, topographic evolution, tectonics, and earthquakes (e.g., He et al., 2014).

The continental lower crust is considered as the bridge between the mostly felsic upper crust and the ultramafic upper mantle (Christensen and Mooney, 1995; Rudnick and Fountain, 1995; Wang et al., 2012). The high density or the ultramafic/mafic composition of the lower crust might lead to instability, resulting in the lower crustal and (or) lithospheric delamination induced by the compressed crust and (or) lithosphere (He et al., 2013, 2014, 2015; Jull and Kelemen, 2001; Kay and Kay, 1993; Kay and Mahlburg-Kay, 1991; Rudnick, 1995; Rudnick and Fountain, 1995; Seber et al., 1996; Willbold and Stracke, 2010). The process of delamination is also important in the cycle of mantle convection, and the heterogeneous lower crustal composition contributes to the variation in mantle velocity structure (Hart, 1988; Hofmann, 1997; Wang et al., 2013).

Geological investigations have suggested large-scale delamination of the crust and lithosphere following the convergence between the Yangtze, North China Cratons and the North Tibetan continental blocks in the Triassic (Zhang et al., 2008), with the delaminated lower crust and lithosphere gradually sinking into the mantle transition zone. The large-scale high-velocity perturbation at the mantle transition zone (Hv3) (Fig. 3, 4a–c, and 5) beneath the NNSTZ might be linked with the crustal and lithospheric delamination in the Triassic, which resulted in a cold domain there, as suggested by the shallowing of both the 410- and 660-km discontinuities (Fig. 6) (He et al., 2014). The crustal and lithospheric components undergo melting in this region, which trigger plume-like upwelling due to buoyancy reflected as low-velocity structure (Lustrino, 2005) (Lv2) (Fig. 3, Fig. 4c, Fig. 5f). On the other hand, the westward subduction or compression of the Pacific plate in the NNSTZ generated an obvious gradient in crustal thickness (Fig. 7a) since the Mesozoic (He et al., 2014), leading to continuing crustal and (or) lithospheric delamination in this area. The high-velocity perturbation at 300–400 km in depth (Hv2) (Fig. 3, Fig. 4d and Fig. 5) is shallower than that of Hv3 (Fig. 3, Fig. 4a–c and Fig. 5), which might indicate new delamination beneath this area. The delamination also induces asthenosphere upwelling into the void (He et al., 2014; Kay and Kay, 1993). Our results suggest that the delamination, both past and present, in the area generates vertical convective circulation of the upper mantle (He et al., 2014). The delamination of the lower crust and lithosphere also resulted in felsic composition of the lower crust (or low Vp/Vs ratios) in the NNSTZ (Fig. 7b) (He et al., 2014; Kay and Kay, 1993).

Previous seismic studies reveal that the lithosphere–asthenosphere boundary lies at a depth of 125–135 km beneath the northeastern Songpan–Ganzi terrane and the western Qinling orogen, between 145 and 175 km beneath the East Kunlun and Qilian orogens, between 175 and 190 km beneath the Qaidam Basin, about 170 km beneath the Ordos Basin and about 200 km beneath the Alxa platform (Zhang et al., 2012; Zheng et al., 2013), respectively. These results suggest the existence of a lithospheric root in the western side of the NNSTZ. However, our results show a large-scale low-velocity perturbation (Lv1) in this region (Fig. 3, Fig. 4a–d), which might suggest that the lithospheric root is weak or absent

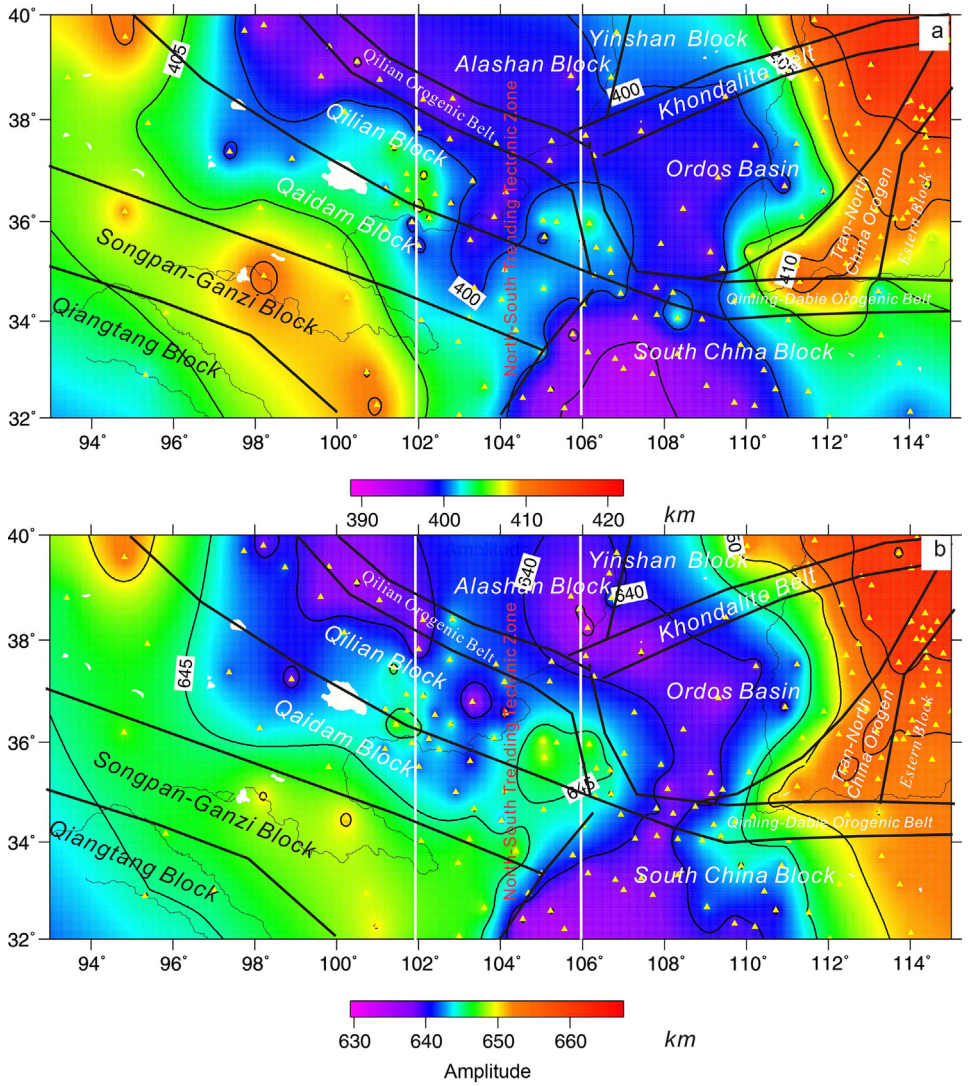

Fig. 6. Topography of the 410 and 660 km discontinuities. A prominent shallowing of both 410 (a) and 660 km (b) topography along the NNSTZ can be seen, possibly correlated with crustal and (or) lithospheric delamination into the mantle transition zone and the resulting cold domain (He et al., 2014).

and also mark the eastward flow from Tibetan plateau. At the eastern side of the NNSTZ, the high-velocity perturbation (Hv1) (Fig. 3, Fig. 4b–d) correlates with the lithospheric root of the Ordos basin and/or that of the Yangtze block (Sichuan basin), which might block the eastward flow from the Tibet Plateau and resulted in stress accumulation at the NNSTZ. At same time, the marked difference in the velocity structure of the lithosphere between the two sides of the NNSTZ implies that there might be not only stress accumulation but also material exchange between the two sides of the NNSTZ, leading to the generation of earthquakes in the NNSTZ.

5. Conclusions

The tomographic results presented in this study confirm the deductions from a previous receiver function study that the delamination of the crust and (or) lithosphere resulted in the mantle upwelling and vertical convective circulation beneath the NNSTZ.

Our results also reveal low-velocity perturbation in the western side of the NNSTZ and high-velocity perturbation in the eastern side on a lithospheric scale, suggesting material exchange and stress accumulation leading to earthquakes beneath this region.

Based on the above results, we suggest that the vertical convective circulation and the velocity perturbation difference in the lithospheric scale between the two flanks of the NNSTZ resulted in stress accumulation and release along this zone, marking the region as earthquake-prone.

The NNSTZ appears to represent a typical case where deformation and the associated tectonic processes trigger large earthquakes, which are associated with mantle

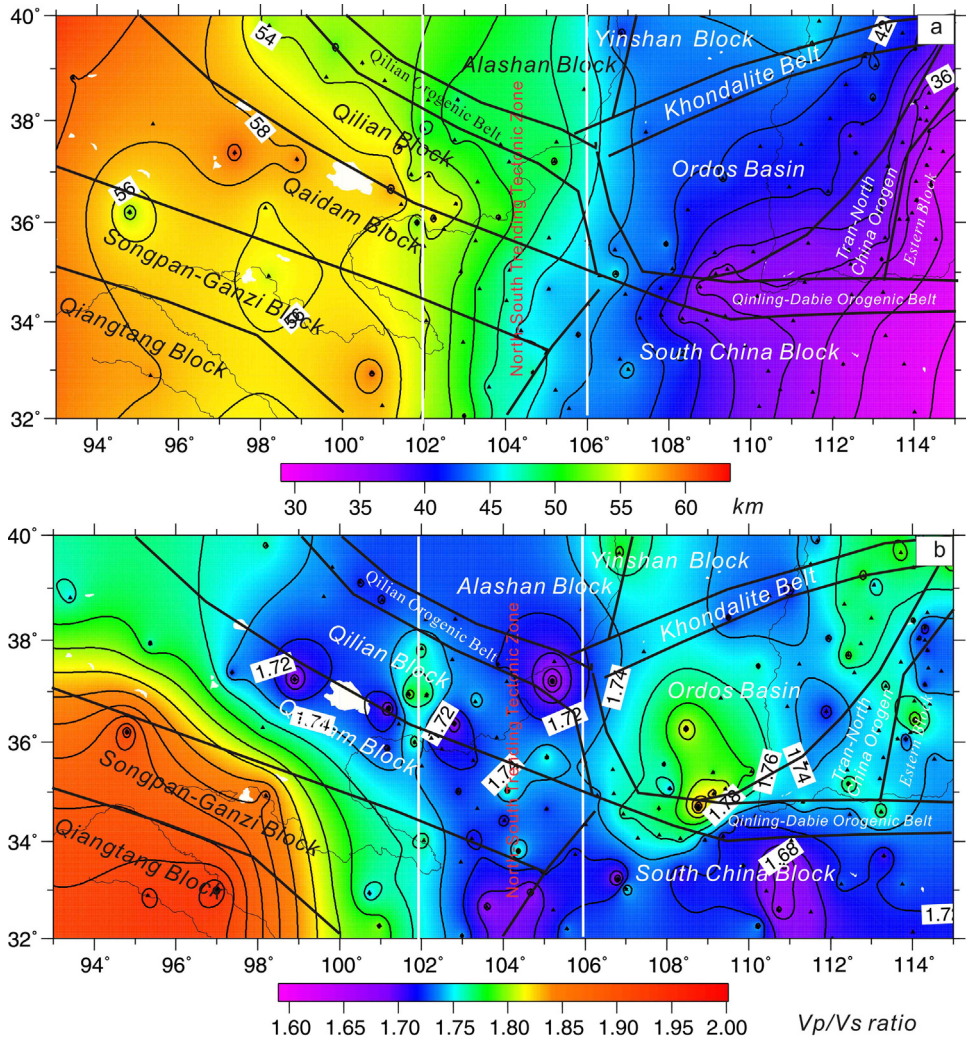

Fig. 7. Distribution of crustal thickness (a) and Vp/Vs ratio (b). A west–east-trending prominent gradient of crustal thickness along the NNSTZ (a) and a prominent low Vp/Vs ratio along the NNSTZ (b) imply that the NNSTZ underwent later crustal delamination (He et al., 2014).

dynamics within intra-continental setting related to far-field tectonics.

Acknowledgements

We thank associate editor M. Campillo, and the two referees Prof. Wenjiao Xiao and Prof. Yanghua Wang for their constructive comments. We thank Prof. D. Zhao, who offered the source codes for tomography. We are also thankful to the guidance and constructive comments of Prof. Shunping Pei. The waveform data for this study were provided by Data Management Centre of China National Seismic Network at Institute of Geophysics (SEISDMC, http://dx.doi.org/10.11998/SeisDmc/SN), China Earthquake Networks Center and GS, GX, NX, QH, SC, XZ Seismic Networks, China Earthquake Administration (Zheng et al., 2010). This study contributes to the Foreign Expert funding from China University of Geosciences, Beijing, and Professorial support from the University of Adelaide to M. Santosh.

Appendix A. Supplementary data

Supplementary data associated with this article can be found, in the online version, at http://dx.doi.org/10.1016/j.crte.2017.04.002.

References

Ames, L., Zhou, G., Xiong, B., 1996. Geochronology and isotopic character of ultrahigh-pressure metamorphism with implications for collision of the Sino-Korean and Yangtze cratons, central China. Tectonics 15, 472–489.

Aitken, A.R.A., Romando, T., Capitano, F.A., 2013. The intraplate character of supercontinent tectonics. Gondwana Res. 24, 807–814.

Bian, Q.T., Li, D.H., Pospelov, I., Yin, L.M., Li, H.S., Zhao, D.S., Chang, C.F., Luo, X.Q., Gao, S.L., Astrakhantsev, O., Chamov, N., 2004. Age, geochemistry

and tectonic setting of Buqingshan ophiolites, North Qinghai–Tibet Plateau, China. J. Asian Earth Sci. 23, 577–596.
Christensen, N.I., Mooney, W.D., 1995. Seismic velocity structure and composition of the continental crust: a global view. J. Geophys. Res. 100, 9761–9788.
Dan, W., Li, X.H., Guo, J.H., Liu, Y., Wang, X.C., 2012. Paleoproterozoic evolution in the eastern Alxa Block, westernmost North China: Evidence from in situ zircon U-Pb dating and Hf-O isotopes. Gondwana Res. 21, 838–864.
Data Management Centre of China National Seismic Network, 2007. Waveform data of China National Seismic Network. Institute of Geophysics, China Earthquake Administration http://www.seisdmc.ac.cn, doi:10.11998/SeisDMC/SN.
Deng, Q., Zhang, P., Ran, Y., Yang, X., Min, W., Chu, Q., 2003. Basic characteristics of active tectonics of China. Sci China C Life Sci 46, 356–372, http://dx.doi.org/10.1360/03yd9032.
Ding, Z.F., He, Z.Q., Sun, W.G., Sun, H.C., 1999. 3-D crustal and upper mantle velocity structure in eastern Tibetan plateau and its surrounding area. Chin. J. Geophys. 42, 197–205.
Eberhart-Phillips, D., 1986. Three-dimensional velocity structure in Northern California Coast Ranges from inversion of local earthquake arrival times. Bull. Seismol. Soc. Am. 76, 1025–1052.
Gao, R., Wang, H.Y., Ma, Y.S., Zhu, X., Li, Q.S., Li, P.W., Kuang, Z.Y., Lu, Z.W., 2006. Tectonic Relationships between the Zoigê Basin of the Song-Pan Block and the West Qinling Orogen at Lithosphere scale: Results of Deep Seismic Reflection Profiling. Acta Geoscientifica Sinica 27, 411–418.
Gorczyk, W., Vogt, K., 2015. Tectonics and melting in intra-continental settings. Gondwana Res. 27, 196–208.
Hart, S.R., 1988. Heterogeneous mantle domains: signatures, genesis and mixing chronologies. Earth Planet. Sci. Lett. 90, 273–296.
He, C.S., Dong, S.W., Santosh, M., Chen, X.H., 2013. Seismic Evidence for a Geosuture between the Yangtze and Cathaysia Blocks, South China. Scientific Reports 3 , http://dx.doi.org/10.1038/srep02200.
He, C.S., Santosh, M., Chen, X.H., Li, X.Y., 2014. Continental dynamics in a multi-convergent regime: a receiver function study from the North–South-Trending Tectonic Zone of China. Internat. Geol. Rev. 56, 525–536, http://dx.doi.org/10.1080/00206814.2013.876901.
He, C.S., Santosh, M., Yang, Q.Y., 2015. Gold metallogeny associated with craton destruction: a geophysical perspective from the North China craton. Ore Geol. Rev, http://dx.doi.org/10.1016/j.oregeorev.2015.12.004.
Hofmann, A.W., 1997. Mantle geochemistry: the message from oceanic volcanism. Nature 385, 219–229.
Huang, Z.C., Wang, P., Xu, M.J., Wang, L.S., Ding, Z.F., Wu, Y., Xu, M.J., Mi, N., Yu, D.Y., Li, H., 2015. Mantle structure and dynamics beneath SE Tibet revealed by new seismic images. Earth Planet. Sci. Lett. 411, 100–111.
Jiang, G.M., Zhang, G.B., Zhao, D., Lü, Q.T., Li, H.Y., Li, X.F., 2015. Mantle dynamics and Cretaceous magmatism in East-Central China: Insight from teleseismic tomograms. Tectonophysics 664, 256–268.
Jiang, G.M., Zhao, D.P., Zhang, G.B., 2009. Crustal correction in teleseismic tomography and its application. Chin. J. Geophys. 52, 1508–1514.
Jull, M., Kelemen, P.B., 2001. On the conditions for lower crustal convective instability. J. Geophys. Res. 106, 6423–6446.
Kay, R.W., Kay, S.M., 1993. Delamination and delamination magmatism. Tectonophysics 219, 177–189.
Kay, R.W., Mahlburg-Kay, S., 1991. Creation and destruction of lower continental crust. Geol. Rundschau 80, 259–278.
Kennett, B., Engdahl, E., 1991. Traveltimes for global earthquake location and phase identification. Geophys. J. Int. 105 (2), 429–465, http://dx.doi.org/10.1111/j.1365-246X.1991.tb06724.x.
Laske, G., Masters, G., Ma, Z., Pasyanos, M.E., 2012. CRUST1.0: an updated global model of Earth's Crust. Geophys. Res. Abstr. 14, (EGU2012-37431).
Lei, J., Zhao, D., 2007. Teleseismic P-wave tomography and the upper mantle structure of the central Tien Shan orogenic belt. Physics of the Earth and Planet. Interiors 162, 165–185.
Li, C., van der Hilst, R.D., Toksöoz, M.N., 2006. Constraining *P*-wave velocity variations in the upper mantle beneath Southeast Asia. Physics of the Earth and Planet. Interiors 154, 180–195.
Li, D.S., 1996. Basic characteristics of oil and gas basins in China. J. South-East Asian Earth Sci. 13, 299–304.
Li, S.L., Zhang, X.K., Zhang, C.K., Zhao, J.R., Cheng, S.X., 2002. A Preliminary Study on Crustal Velocity Structures of Maqin-Lanzhou-Jingbian Deep Seismic Sounding Profile. Chin. J. Geophys. 45, 209–216.
Liu, J.H., Liu, F.T., Wu, H., Li, Q., Hu, G., 1989. Three dimensional velocity images of the crust and upper mantle beneath north-south zone in China. Chin. J. Geophys. 95, 916–925.
Lustrino, M., 2005. How the delamination and detachment of lower crust can influence basaltic magmatism. Earth Sci. Rev. 72, 21–38.
Paige, C., Saunders, M., 1982. LSQR: An algorithm for sparse linear equations and sparse least squares. Trans. Math. Software 8, 43–47, http://dx.doi.org/10.1145/355984.355989.
Pandey, S., Yuan, X., Debayle, E., Priestley, K., Kind, R., Tilmann, F., Li, X., 2014. A 3D shear-wave velocity model of the upper mantle beneath China and the surrounding areas. Tectonophysics 633, 193–210.
Ratschbacher, L., Hacker, B.R., Webb, L.E., McWilliams, M., Ireland, T., Dong, S., Calvert, A., Chateigner, D., Wenk, H.R., 2000. Exhumation of the ultrahigh-pressure continental crust in East-central China: Cretaceous and Cenozoic unroofing and the Tan-Lu fault. J. Geophys. Res. 105, 13303–13338.
Rudnick, R.L., 1995. Making continental crust. Nature 378, 571–578.
Rudnick, R.L., Fountain, D.M., 1995. Nature and composition of the continental crust: a lower crustal perspective. Rev. Geophys. 33, 267–309.
Santosh, M., 2010. Assembling North China Craton within the Columbia supercontinent: The role of double-sided subduction. Precambrian Res. 178, 149–167.
Santosh, M., Liu, D.Y., Shi, Y.R., Liu, S.J., 2013. Paleoproterozoic accretionary orogenesis in the North China Craton: A SHRIMP zircon study. Precambrian Res. 227, 29–54.
Santosh, M., Wilde, S.A., Li, J.H., 2007. Timing of Paleoproterozoic ultrahigh temperature metamorphism in the North China Craton: evidence from SHRIMP U-Pb zircon geochronology. Precambrian Res. 159, 178–196.
Seber, D., Barazangi, M., Ibenbrahim, A., Demnati, A., 1996. Geophysical evidence for lithospheric delamination beneath the Alboran Sea and Rif-Betic mountains. Nature 379, 785–790.
Song, S.G., Su, L., Li, X.H., Zhang, G.B., Niu, Y.L., Zhang, L.F., 2010. Tracing the 850-Ma continental flood basalts from a piece of subducted continental crust in the North Qaidam UHPM belt, NW China. Precambrian Res. 183, 805–816.
Tian, Y., Zhao, D., Sun, R., Teng, J.W., 2009. Seismic imaging of the crust and upper mantle beneath the North China Craton. Physics of the Earth and Planet. Interiors 172, 169–182.
Tseng, C.Y., Yang, H.J., Yang, H.Y., Liu, D.Y., Wu, C.L., Cheng, C.K., Chen, C.H., Ker, C.M., 2009. Continuity of the North Qilian and North Qinling orogenic belts, Central Orogenic System of China: Evidence from newly discovered Paleozoic adakitic rocks. Gondwana Res. 16, 285–293.
Tung, K.A., Yang, H.J., Yang, H.Y., Liu, D., Zhang, J., Wan, Y., Tseng, C.Y., 2007. SHRIMP U–Pb geochronology of the zircons from the Precambrian basement of the Qilian block and its geological significances. Chin. Sci. Bull 19, 2687–2701.
Wang, C.Y., Flesch, L.M., Silver, P.G., Chang, L.J., Chan, W.W., 2008. Evidence for mechanically coupled lithosphere in central Asia and resulting implications. Geology 36, 363–436.
Wang, C.Y., Yang, W.C., Wu, J.P., Ding, Z.F., 2015. Study on the lithospheric structure and earthquake in North–South Tectonic belt. Chin. J. Geophys. 58, 3867–3901.
Wang, J., Zhao, D., 2013. P-wave tomography for 3-D radial and azimuthal anisotropy of Tohoku and Kyushu subduction zones. Geophys. J. Int. 193, 1166–1181.
Wang, S., Niu, F., Zhang, G., 2013. Velocity structure of the uppermost mantle beneath East Asia from Pn tomography and its dynamic implications. J. Geophys. Res. Solid Earth 118, 290–301.
Wang, Y.F., Zhang, J.F., Jin, Z.M., GreenII, H.W., 2012. Mafic granulite rheology: Implications for a weak continental lower crust. Earth Planet. Sci. Lett. 353–354, 99–107.
Wang, Y.H., Houseman, G.A., Lin, G., Guo, F., Wang, Y.J., Fan, W.M., Chang, X., 2005. Mesozoic lithospheric deformation in the North China block: Numerical simulation of evolution from orogenic belt to extensional basin system. Tectonophysics 405, 47–63.
Willbold, M., Stracke, A., 2010. Formation of enriched mantle components by recycling of upper and lower continental crust. Chem. Geol. 276, 188–197.
Xiao, W.J., Windley, B.F., Sun, S., Li, J.L., Huang, B.C., Han, C.M., Yuan, C., Sun, M., Chen, H.L., 2015. A tale of amalgamation of three collage systems in the Permian-Middle Triassic in central Asia: Oroclines, sutures and terminal accretion. Ann. Rev. Earth Planet. Sci., 43, 477-507, http://dx.doi.org/10.1146/annurev-earth-060614-105254.
Xu, Y.J., Du, Y.S., Cawood, P.A., Yang, J.H., 2010. Provenance record of a foreland basin: Detrital zircon U–Pb ages from Devonian strata in the North Qilian Orogenic Belt, China. Tectonophysics 495, 337–347.
Xu, Z.Q., Yang, J.S., Wu, C.L., Li, H.B., Zhang, J.X., Qi, X.X., Song, S.G., Qiu, H.J., 2006. Timing and mechanism of formation and exhumation of the northern Qaidam ultrahigh-pressure metamorphic belt. J. Asian Earth Sci. 28, 160–173.
Yang, T., Wu, J.P., Wang, W.L., 2014. Complex Structure beneath the southeastern Tibetan Plateau from Teleseismic P-Wave Tomography. Bull. Seismol. Soc. Am. 104, 1056–1069.

Yin, A., Nie, S., 1996. A Phanerozoic palinspastic reconstruction of China and its neighboring region. In: Yin, A., Harrison, T.M. (Eds.), The Tectonic Evolution of Asia. Cambridge University, New York, pp. 442–485.

Zhang, C.Z., Li, B., Cai, J.X., Tang, X.C., Wei, Q.G., Zhang, Y.X., 2008. A-type granite and adakitic magmatism association in Songpan-Garze fold belt, eastern Tibetan Plateau: Implication for lithospheric delamination. Lithos 103, 562–564.

Zhang, G.W., Guo, A.L., Wang, Y.J., Li, S.Z., Dong, Y.P., Liu, S.F., He, D.F., Cheng, S.Y., Lu, R.K., Yao, A.P., 2013. Tectonics of South China continent and its implications. Sci. China Earth Sci. 56 (11), 1804–1828.

Zhang, H.S., Teng, J.W., Tian, X.B., Zhang, Z.J., Gao, R., Liu, J.Q., 2012. Lithospheric thickness and upper-mantle deformation beneath the NE Tibetan Plateau inferred from S receiver functions and SKS splitting measurements. Geophys. J. Int., http://dx.doi.org/10.1111/j.1365-246X.2012.05667.x.

Zhang, P.Z., Deng, Q., Zhang, G., Ma, J., Gan, W., 2003. Active tectonic blocks and strong earthquakes in continental China. Sci China C Life Sci 33, 13–24 (Suppl).

Zhang, X., Wang, Y.H., 2009. Crustal and upper mantle velocity structure in Yunnan, Southwest China. Tectonophysics 471, 171–185.

Zhao, D., Hasegawa, A., Horiuchi, S., 1992. Tomographic imaging of P and S wave velocity structure beneath northeastern Japan. J. Geophys. Res. 97, 19909–19928, http://dx.doi.org/10.1029/92JB00603.

Zhao, D., Hasegawa, A., Kanamori, H., 1994. Deep structure of Japan subduction zone as derived from local, regional, and teleseismic events. J. Geophys. Res. 99, 22313–22329, http://dx.doi.org/10.1029/94JB01149.

Zhao, D., Mishra, O., Sanda, R., 2002. Influence of fluids and magma on earthquakes: Seismological evidence. Phyics of the. Earth Planet. Interiors 132 (4), 249–267, http://dx.doi.org/10.1016/S0031-9201(02)00082-1.

Zhao, G.C., Sun, M., Wilde, S.A., Li, S.Z., 2005. Late Archean to Paleoproterozoic evolution of the North China Craton: key issues revisited. Precambrian Res. 136, 177–202.

Zhao, G.C., Wilde, S.A., Guo, J.H., Cawood, P.A., Sun, M., Li, X.P., 2010. Single zircon grains record two Paleoproterozoic collisional events in the North China Craton. Precambrian Res. 177, 266–276.

Zheng, X.F., Yao, Z.X., Liang, J.H., Zheng, J., 2010. The role played and opportunities provided by IGP DMC of China National Seismic Network in Wenchuan earthquake disaster relief and researches. Bull. Seismol. Soc. Am. 100 (5B), 2866–2872, http://dx.doi.org/10.1785/0120090257.

Zheng, Y.F., Xiao, W.J., Zhao, G.C., 2013. Introduction to tectonics of China. Gondwana Res. 23, 1189–1206.